

Buzz Simulation on a Supersonic Transport Configuration

A. M. Rampurawala and K. J. Badcock

CFD Laboratory, Department of Aerospace Engineering,

University of Glasgow, Glasgow G12 8QQ, U.K.

email: amoosa@aero.gla.ac.uk

Keywords: Buzz, control surfaces, aeroelasticity.

Abstract This paper describes a buzz simulation performed on a Japanese Supersonic Transport (SST) configuration. The SST wing profiles are characterised by a small wing thickness optimised for operation in supersonic cruise conditions. Due to the thinness of the wing there is limited space for constraints of the control surfaces at the trailing edge making them susceptible to a buzz instability in transonic conditions. In the current work an FEM structural model is constructed and analysed for natural modes and frequencies using NASTRAN. A flap is attached to the wing with a spring attachment and its oscillation controlled by adjusting the spring stiffness. 3D buzz simulation is performed using the Glasgow University multiblock CFD code PMB. Characteristics of buzz first noticed in experiments and 2D simulations are observed. Two types of flap treatment for CFD based calculations are used to simulate buzz and the results compared. Effect of buzz on the flutter boundary is also investigated and compared with flutter results obtained from NASTRAN. The wing bending and torsion frequencies are similar to the those obtained from a GVT test and the flap mode is included to see the effect it has on the flutter speed.

NOMENCLATURE

Symbols

c_r	wing root chord = 2.103 metres
\mathbf{f}	force acting at the grid points
\mathbf{K}	structural stiffness matrix
k	reduced frequency $\frac{2\pi\omega c_r}{u_\infty}$
\mathbf{M}	structural mass matrix
t	real time
u_∞	freestream velocity in m/s
x, y, z	Cartesian coordinates
x_t, y_t, z_t	fluid grid speeds
\mathbf{x}	grid locations

Greek

η	generalised modal coordinates
ω	modal frequency in Hz

ϕ	mode shape
ψ_i^0	Blending function for Transfinite Interpolation
ρ	fluid density

Subscripts

a	aerodynamic surface grid
s	structural grid

Superscripts

n	time level
---	------------

1 INTRODUCTION

In recent years Computational Aeroelasticity (CAE) has advanced to a point where flutter boundaries for complete aircraft configurations can be predicted, even in the difficult transonic flow regime^{1,2,3,4}. Along with simulations of classical aeroelastic instabilities like flutter and divergence, an interesting area of CAE application is the prediction of control surface instabilities like buzz. Detailed work on numerical simulations of buzz has not been undertaken mainly because by the time the computational tools were in place for such an undertaking, buzz ceased to be an issue in modern aircraft. The advent of hydraulic actuators prevented the control surfaces from developing oscillation along its hinge in contrast to flaps on older aircraft with mechanical spring loaded fixtures. Experimentally there were a number of important studies in 60s and 70s exploring the buzz phenomenon.^{5,6,7}

The popular classification of buzz in the literature was defined by Lambourne.⁵ During the course of his experiments he found that there were 3 main types of buzz possible on a trailing edge flap configuration, which he called Type A, Type B and Type C buzz. Type A buzz occurs when the shock stands somewhere ahead of the flap hinge line and interacts with the boundary layer and the flap motion. The limit cycle oscillation is brought about by the synchronisation of the shock strength and motion, the flow separation and the angular flap motion. As the control surface moves it alternately weakens or strengthens the shock, causing separation and reattachment of the flow. The separated flow in turn creates a hinge moment at the flap leading edge which makes the flap undergo oscillation. The Type A buzz is limited to thick aerofoils and is rarely seen in aerofoils having less than 10% camber.⁸ Shock induced flow separation is the primary requirement for Type A buzz to occur. Type B buzz as classified by Lambourne is when the shock crosses the hinge line and translates over the control surface. The driving mechanism here is the unsteady hinge moment from the pressure pulse created by the shock motion. The hinge moments involved in Type B buzz are greater than in Type A and are much more difficult to alleviate. In terms of numerical simulation Type B buzz can be simulated using the Euler equations. An accurate buzz boundary can be defined using the Euler equations if some empirically based action is taken to correct the mean shock location. Although there is flow separation over the flap in Type B buzz which can effect the amplitude and frequency of the buzz, the actual onset of buzz is not influenced.⁸ Type C buzz occurs when the shock has crossed the whole length of the control surface and is attached to the trailing edge. This type of buzz occurs in upper supersonic flows and is thought not to involve flow separation.

Until now there have been few numerical simulations of buzz described in the literature. One of the

first such studies was performed by Steger⁹ who carried out a 2D buzz simulation on a P-80 wing using an implicit finite difference code capable of solving the RANS equations. The P-80 aircraft was already known to suffer from buzz problems during flight testing and this was further investigated in the NASA Ames wind tunnel by Erickson and Stephenson¹⁰. Steger was able to match the computed results with the experiments and also measured the effect of viscosity on buzz simulations. It was found that for a certain Mach number the oscillations in an inviscid calculation would die down after an initial kick but that the oscillations in viscous simulations would result in a limit cycle.⁹ At another higher Mach number the inviscid simulation would diverge whereas the RANS simulation would still predict a limit cycle. Hence he deduced that viscosity had an effect of both preserving and mitigating the oscillations. Fuglsang *et al.*¹¹ solved a buzz problem on the fin-rudder section of T-45 Goshawk aircraft through steady CFD simulations. By analysing the flow field using CFD at around the flow parameters where buzz was known, a solution using 2 parallel shock strips was developed. Shock strips are raised sections that are stuck on the wing to move the shock forward of its normal position. The strips were successful in alleviating buzz on the T-45 flight envelope. Bendiksen numerically investigated a type of buzz instability that relies purely on interaction between the shock and flap motion, which he termed non-classical buzz.⁸ He showed that for certain cases, especially for thin aerofoil sections, the flow separation does not play an important role in maintaining a limit cycle oscillation. A good comparison of a buzz boundary traced from inviscid calculations with experiments was obtained.⁸ Recently the non-harmonic motion of the shock over an aerofoil with a harmonically oscillating flap¹² and 3D aileron buzz using thin layered RANS equations were shown.¹³ The oscillations of the control surface, forced or otherwise, causes a flexible aircraft structure to deform due to the unsteady redistribution of the surface pressure. This may lead to a decrease in the flutter velocity and hence analysis of control surface effects on the overall aeroelastic behaviour is important for some configurations. The above findings form the starting point for this work which aims to predict 3D buzz of a supersonic aircraft configuration and the effect of the flap on the flutter boundary.

The Japan Aerospace Exploration Agency¹ (JAXA) has been developing scaled powered and non-powered Supersonic Transport aircraft as part of their objective to acquire and establish advanced aircraft integration technology. The first non-powered model from this program was launched in Woomera, Australia in 2002. As with all supersonic configurations this model had thin low aspect ratio wings with little possibility of flow separating over the wing at moderate angles of attack within the flight envelope. However at high transonic and low supersonic regions a strong shock will develop over the trailing edge where a trailing edge flap/aileron might be situated. Due to the thinness of a supersonic wing it is difficult to have stiff hinges or powered actuating systems or at the trailing edge flap. This means that the shock motion over the flap can interact with the flexible one degree of freedom flap by feeding energy to it and causing undamped flap oscillations that grow in time.

As the wings used for supersonic aircraft are usually thin, analysis for Type B buzz is of most relevance. In the current work a Type B buzz is simulated using both RANS and Euler equations on a 3D SST configuration. A brief description of the CAE methodology used for this work is given in Section 2. Section 3 explains the methods used for modelling the flap in CFD based simulations. Section 4 describes the geometry, the structural model and the CFD grids used. Section 5 discusses the results obtained from the simulations including effects of various parameters on buzz. The effect of flap on the flutter velocity is also investigated in this section. Finally some conclusions are drawn from the current work in Section 6.

¹formerly National Aerospace Laboratory (NAL)

2 CAE Methodology

All computations were performed using the Parallel Multi-Block (PMB) flow solver¹⁴ developed at the University of Glasgow, which has been continually revised and updated over a number of years. The solver has been successfully applied to a variety of problems including cavity flows, hypersonic film cooling, spiked bodies, flutter and delta wing flows amongst others. The fluid and structural equations are solved on separate grids. The aerodynamic force is calculated over the fluid surface grid and is interpolated to the structural grid using the Constant Volume Tetrahedron (CVT) transformation scheme.¹⁵ The deformation on the structural grid is calculated using the modal FEM solver and the fluid surface grid is updated using the latest deformation. To minimise the sequencing errors the fluid and structural equations are coupled in pseudo time.¹⁶

2.1 CFD solver

The code solves the unsteady Reynolds Averaged Navier-Stokes equations, in serial or parallel mode on multi-block structured grids. Governing equations are discretised using a cell-centred finite volume method. The convective terms are discretised using either Osher's or Roe's scheme. MUSCL interpolation is used to provide nominally third order accuracy and the Van Albada limiter is used to avoid spurious oscillations across shocks. The time-marching of the solution is based on an implicit, dual time-stepping method. The final algebraic system of equations is solved using a Conjugate Gradient method, in conjunction with Block Incomplete Lower-Upper factorisation. A number of turbulence models including one and two-equation statistical models as well as Large-Eddy Simulation (LES) and Detached Simulation (DES) formulations have been implemented into the code. More details on the PMB solver can be found in Badcock et. al.¹⁴ In the current work the $k - \omega$ turbulence model was used for all the viscous calculations.

2.2 Structural solver

Finite element methods allow for the static and dynamic response of a structure to be determined. Stiffness (\mathbf{K}) and mass (\mathbf{M}) matrices are used to determine the equation of motion of an elastic structure subjected to an external force \mathbf{f}_s as

$$\mathbf{M}\delta\ddot{\mathbf{x}}_s + \mathbf{K}\delta\mathbf{x}_s = \mathbf{f}_s \quad (1)$$

where $\delta\mathbf{x}_s$ is a vector of displacements on a grid of points \mathbf{x}_s . Because the structural system under consideration is assumed to be linear, its characteristics are determined once and for all prior to making the flutter calculations, so that \mathbf{M} and \mathbf{K} are constant matrices generated, in this case, by the commercial package NASTRAN.

The aircraft deflections $\delta\mathbf{x}_s$ are defined at a set of grid points \mathbf{x}_s by

$$\delta\mathbf{x}_s = \sum \eta_i \phi_i \quad (2)$$

where ϕ_i are the mode shapes and η_i the generalised displacements. Here the η_i depend on time but the mode shapes do not. The values of ϕ_i and ω_i are calculated by solving the eigenvalue problem

$$[\mathbf{M} - \omega_i^2 \mathbf{K}]\phi_i = \mathbf{0}. \quad (3)$$

The eigenvectors are scaled so that

$$[\phi_i]^T \mathbf{M} [\phi_i] = 1. \quad (4)$$

Projecting the finite element equations onto the mode shapes results in the equations

$$\frac{d^2\eta_i}{dt^2} + \omega_i^2\eta_i = \phi_i^T \mathbf{f}_s \quad (5)$$

where \mathbf{f}_s is the vector of external forces at the structural grid points. This equation can be solved by a two stage Runge-Kutta method, which requires a knowledge of \mathbf{f}_s^n and \mathbf{f}_s^{n+1} . To avoid introducing sequencing errors by approximating the term \mathbf{f}_s^{n+1} the Runge-Kutta solution is iterated in pseudo time along with the fluid solution i.e. the latest estimate for \mathbf{f}_s^{n+1} is used in the Runge Kutta solution. At convergence of the pseudo time iterations the structural and fluid solutions are properly sequenced in time. It should be noted that the cost of the coupled calculation resides with the CFD solver when modal structural models are used. The CFD solver used in the current work is of good efficiency in the sense that the time step is always chosen to adequately resolve the solution temporally and is never chosen to facilitate the operation of the solver due to stability or any other numerical considerations.

2.3 Mesh movement

The geometries of interest deform during the motion and the mesh must be moved to conform with the evolving geometry. This is achieved using Transfinite Interpolation (TFI) of displacements within the blocks containing the aircraft. The surface deflections are interpolated to the volume grid points \mathbf{x}_{ijk} as

$$\delta\mathbf{x}_{ijk} = \psi_j^0 \delta\mathbf{x}_{a,ik} \quad (6)$$

where ψ_j^0 are values of a blending function¹⁷ which varies between one at the aircraft surface and zero at the block face opposite. The surface deflections $\mathbf{x}_{a,ik}$ are obtained from the transformation of the deflections on the structural grid and so ultimately depend on the values of the generalised structural coordinate η_i . The grid speeds can be obtained by differentiating equation (6) to obtain their explicit dependence on the values of $\dot{\eta}_i$.

3 FLAP TREATMENT

Computational simulations involving moving control surfaces are still not common mainly due to the difficulty in treating the grid over and around the control surfaces. The free edges of the flap causes geometrical discontinuity along the wing span which is difficult to cope within the framework of a multiblock code. There are a number of ways a 3D flap can be modelled in a multiblock environment, the most simple being the blending of inboard and outboard edges of the flap with the wing surface. The blending does cause a deviation from the proper representation of the flap geometry but the effect the blending has on flow solution needs to be assessed. Another option for modelling the flap is the introduction of small gaps in between the inboard/outboard flap edges and the wing. When the flap is deflected along its hinge the cells in these gap blocks are sheared. A flap modelled in this way maintains its geometric details but there is a penalty to be paid in the computational time as the grid quality inside the sheared gap blocks is poor. There are other more complex options that would require changes in the multiblock flow code itself like sliding planes¹⁸ and a virtual zone technique for control surfaces,¹⁹ but these are outside the scope of this paper. In this paper the buzz simulation cases are performed using blended flaps, and with gaps used to measure the effect the blending has on the results.

3.1 Blended Flaps

The attractive feature of blending the flaps is the ease with which it can be implemented into a multi-block CFD based calculation while maintaining a reasonable grid quality, even for very large flap deflection angles. This allows RANS calculations to be performed, even when the flap undergoes a large deflection. The blending of inboard and outboard flap edges is carried out using a three level hierarchical blending scheme which is an extension of the two level scheme previously described.²⁰ The blending scheme works by influencing the deformation of a lower hierarchy component by a higher component and the interface nodes are driven by the deformation of the higher hierarchical component. For the flap this means that the inboard and outboard edges are driven by the wing and the flap nodes adjacent to the edge nodes are driven by a combination of wing and flap deformations. The extent of the influence of the wing on the flap depends on the blending parameter,²⁰ hence the choice of the blending parameter controls the extent of blended length of the flap. Figure 1 shows a blended flap deflected by 20° using two different values of blending parameters.

3.2 Flaps with Free Edges

This type of flap modelling is more representative of the actual flap geometry but suffers from poor grid quality within the gap blocks, especially when the amplitude of flap deflection is large. The basic idea is to insert gaps between the inboard and outboard edges of the flap. These gaps contain a grid block in which the cells are sheared when the flap rotates around the hinge. In the current work each gap has a width of 0.5% of the total flap span. Figure 2 shows the flap deflected by 20° .

4 MODELS AND GRIDS

4.1 The CAD Model

The geometry of the configuration is as described in the RTO report-26.²¹ The section profile is a NACA 0003 and the wing is a cranked double delta. A fuselage swell near the wing trailing edge, which was present in the experimental model to house the flap oscillation mechanism, is eliminated from the CAD model. The wing tip is modelled by rotating the aerofoil at the tip.

4.2 The Structural Model

The structure of the SST was modelled as a 2D plate in NASTRAN with the aid of the PATRAN preprocessor. The flap is modelled as a separate plate attached to the main wing through springs (See Figure 3). Two structural models were constructed using the same material and geometric properties. The difference between the two models is in the value of the spring stiffness at the flap hinge. The spring stiffness constant in Model 1 is adjusted so that it gives a flap frequency of 16.2 Hz which is within the realistic frequency range of a mechanically constrained trailing edge control surface. The spring stiffness constant of the hinge in Model 2 is set very high so that the flap is constrained and the flap mode is eliminated. The first computed natural mode of vibration is a wing bending mode that has the frequency similar to the previous values.²¹ Table 1 gives the details of the natural frequencies of the 2 models used in the buzz and flutter calculations. The second natural mode of Model 1 is the flap oscillation mode which is used for buzz simulations. The first 5 natural modes were used for flutter calculations for the case with the flap having a low hinge spring attachment stiffness and the first 4 natural modes were used in flutter calculations for the case with a high hinge spring attachment stiffness. By increasing the stiffness of the flap hinge the flap oscillation mode was eliminated at the

same time maintaining the shape and frequencies of other modes. The wing structure is made up of 550 triangular elements and the flap has 20 elements. The fuselage structure consists of two triangular elements that are clamped rigid.

4.3 CFD Grids

To model the effect of gaps and viscosity a total of 4 different grids have been used in this work. The viscous grid has 15 cells to resolve the boundary layer. The wall spacing is of 1.8×10^{-6} chord lengths. The viscous calculations are performed only with blended flaps as there are problems with grid quality when gaps are introduced at flap edges. A C-Type grid topology is used over the wing leading edge, the wing tip and also around the fuselage. The blocks at the trailing edge are of H-Type. The C-Type blocks wrap around the rounded leading edge and the tip ensuring orthogonal cells which otherwise would be not possible with an H-H Type of blocking. The wing geometry is basically a slender delta wing on the inboard side and a collapsed triangular block is avoided at the leading edge tip by using a 3-block strategy as shown in Figure 4. Points are clustered around the trailing edge and the flap region where the shock is likely to develop and move during the buzz simulation. There are 14 cells in the chordwise direction and 28 in spanwise direction on the flap. The size of the viscous grid is 800k cells. The grid is capable of accurately resolving the flow in the region of interest but at the same time is small enough to allow rapid turn around for the unsteady calculations. The blended Euler grids have the same topology as the viscous grid. The fine Euler grid has 1.6 million cells. There are 24 cells in the chordwise direction and 50 spanwise. The wall spacing is 1×10^{-3} chord lengths. A coarse grid is obtained from the fine grid by removing every alternate grid point in all the three directions. The coarse Euler grid has 200k cells. The grid used for flaps with gaps is the same as the coarse Euler grid for blended flaps but with two extra blocks inside gaps between the flap edges and the wing.

5 RESULTS AND DISCUSSIONS

The steady and unsteady results for a case with a forced flap motion have been validated with the experiments.²² The current paper deals with a flap that is driven by the unsteady aerodynamics and unlike the previous case experimental results are not available for validation.

5.1 Grid and time Step refinement study

A timestep refinement study was performed on the viscous case at Mach 0.987. At a freestream velocity of $275m/s$ the reduced frequency of the response is 0.778. Figure 5(a) shows the timetraces of the modal response using timesteps of 0.025, 0.05 and 0.1. As can be seen the curves of timesteps 0.025 and 0.05 almost overlap each other and maintain the frequency and the amplitude. Hence a timestep of 0.05 is used for all the buzz simulations in the current study. Figure 5(b) shows the modal response at Mach 0.95 using the Euler calculations on fine and coarse grids with timesteps of 0.05 and 0.1. Once again the modal response curves overlap each other. The results indicate the coarse Euler grid with a timestep of 0.05 are able to adequately predict the flap response.

5.2 Dependence of buzz on flap blending

This section concerns the effect of the blending parameter²⁰ on the onset of buzz. Again a coarse Euler grid is used to measure this effect as we are concerned with the variation in the predicted buzz Mach number with a change in the blending parameter. In the first case a low blending parameter of

20 and in the second a higher blending parameter of 100 is used. The larger the value of the blending parameter the more the transformed fluid grid conforms to the structural grid at the given transformed mode. For the flap mode where the flap nodes move relative to the wing nodes the blending parameter acts as a damper limiting the motion of the flap. This damping effect decreases with the increasing value of the blending parameter. Also a higher blending parameter maintains the proper shape of the flap as shown in Figure 1. The choice of the parameter depends on the dimensions of the flap and shape of the mode. Figure 6 shows the angle against time for the two values of blending parameter. The flap modelled with a blending parameter of 20 has, in general, a more restrained response both in amplitude and in frequency.

The third case is the one with the flap having unblended free edges. There are gaps introduced in the inboard and outboard edges of the flap. The total width of both gaps combined is 1% of the flap span. The cells in these gaps are sheared as the flap moves from its mean position and due to this the flap motion is limited to a smaller amplitude of oscillation when compared to blended flaps. The flow inside the fluid grid blocks of the gap take a longer time to converge due to poor grid quality of the sheared cells and hence increases the overall computation time by almost 50%. In terms of prediction of the Mach number at which buzz occurs the two types of flap treatment give similar results. Table 2 shows the occurrence of buzz at different Mach numbers as predicted by different simulation methods. The angle of incidence for all the cases is 0.6° and the Reynolds number for the viscous case is 21.42 million. It is observed during calculations that the maximum amplitude of flap rotation is at Mach numbers 0.91 - 0.93 with flap rotation angles approaching 25° . The amplitude of flap angle for the blended case is larger than the flap with free edges as seen in Figure 7. This is due to the fact that the blended flap has more surface area for the shock driven unsteady aerodynamics to act on and hence more force is transferred to the structural grid resulting in larger deformations.

A conclusion that can be drawn from Table 2 with respect to Euler and viscous calculations is the dependence of Type-B buzz on the shock prediction. As the Euler equations predict the shock aft of RANS modelled flows for a given angle of incidence and Mach number, hence even the Mach number at which RANS equations predict the onset of Type-B buzz is greater. It was found for the current case that the location of the shock predicted by the Euler equations at Mach 0.98 is the same as the location predicted by the RANS equations at Mach 0.987. Figure 8 shows the pressure contours for the inviscid case at Mach 0.98 and the viscous case at Mach 0.987. The slice is taken at 38.4 % span and the shock locations for both the cases is at approximately 95.7% local chord. The angle of incidence is 0.6° .

5.3 Dependence of buzz on the initial impulse

It is known that control surface buzz is sensitive to the initial "kick" given to it. In cruise conditions this displacement of the control surface can be brought about by atmospheric turbulence or sudden changes in dynamic pressure along the flight path. Depending on the magnitude of the displacement angle of the control surface and the Mach number, a shock can develop over either the upper or lower side of the control surface. Figures 9 and 10 show unsteady pressure contours through a cycle of oscillation that is growing in amplitude. It is an inviscid solution on the fine grid with the wing at an incidence of 0.6° and at a Mach number of 0.95. The slice is taken through 32 % wing span which intersects the flap at 40 % span. The coupled calculation is initiated by perturbing the generalised velocity of the mode. The coupled aeroelastic calculations update the new flap position and the aerodynamic solution at each time step. Depending on the angle the flap makes due to the initial perturbation and the Mach number, the shock can either develop far aft of the flap or remain near the flap leading edge. The strength and position of the displaced shock on the flap decides whether the

system will enter an LCO or if the initial perturbation will die down. Hence the buzz onset depends both on the Mach number and the size of the initial perturbation at a given incidence.

Consider a case where a large initial perturbation is applied as shown in Figures 9 and 10. The side with the shock has an area of higher free stream velocity and hence lower dynamic pressure than the opposite side. This pressure difference above and below the control surface creates a hinge moment that pulls the control surface towards the opposite side weakening the shock. Due to the inertial forces and the lag in the aerodynamic response the control surface continues its motion resulting in the formation of a shock on the opposite side. This cycle continues locking the system into a limit cycle oscillation due to the motion of the shock over the control surface. Figure 12 shows the same case but with a low initial perturbation. Here the initial impulse is not strong enough for the flap to deflect to a required angle for a strong shock to develop over the control surface. Hence the hinge moment created is too weak for the LCO to ensue. Figure 11 shows the dependence of buzz to the initial aerodynamic impulse at different Mach numbers. It can be seen that for low transonic cases, where the shock is not very aft of the hinge line, buzz is dependent on the initial perturbation, but for high transonic and supersonic cases even a small impulse can result in buzz. This phenomenon was also observed in 2D simulations by Bendiksen.⁸ Steger found that buzz was dependent on the initial position of the flap.⁹ The results in Figure 11 are from calculations performed on a coarse grid using Euler equations. As viscous effects are not modelled the instability here is brought about purely due to the motion of the shock. The dependence on the initial impulse is also observed in viscous simulations.

5.4 Dependence of buzz amplitude and frequency on Reynolds numbers

It was shown experimentally⁷ that for lower values of reduced frequency the LCO amplitude was sensitive to the Reynolds number. Figure 13 shows the time traces of the flap amplitude for constant reduced frequencies and dynamic pressure at two different values of Reynolds number. Both the cases in Figure 13(a) and Figure 13(b) have the same dynamic pressure but different reduced frequencies which is achieved by adjusting the freestream density. For both cases the amplitude and the buzz frequency increase slightly with an increase in the Reynolds number. Although it was shown⁷ that the sensitivity to Reynolds number changes was only at low values of reduced frequency, it was observed in the current work that amplitudes were sensitive to the Reynolds number even for higher values of reduced frequency. In the previous work viscous effects are more pronounced on account of the thicker aerofoil profile and bigger flap to wing chord ratio. In the current case the flow, even at a high Reynolds number of 21.42 million, is attached along the entire chord of the wing except at larger flap deflection angles when a separation bubble forms at the flap trailing edge. The size of the bubble varies as the flap oscillates and effects the hinge moments. The separation causes a region of low pressure and this could be the reason why the amplitude increases with the Reynolds number. Figure 14 shows the flow streamlines at Mach 0.987 and an incidence of 0.6° during a buzz cycle when the flap is deflected at 0° and $\pm 14.5^\circ$. From the figure it can be seen that the separation is shock induced and on account of the wing having a small incidence of 0.6° the separation bubble when the flap is down (-14.5°) is a bit larger than the separation bubble formed when the flap is up ($+14.5^\circ$).

5.5 Dependence of buzz amplitude on structural damping

Figure 15 shows the buzz amplitude against percentage structural damping for the Euler case at Mach 0.98 and incidence of 0.6° . The amplitude steadily decreases until it dies suddenly at a structural damping of 24%. The amplitude of oscillation at 23% damping is 5.977° . In contrast to Euler simulations the buzz amplitude is much more sensitive to damping in viscous simulations. Figure 15(b)

shows the amplitude against damping for the viscous case at Mach 0.987. The slope of amplitude versus damping is much more steeper and 13 % damping is enough to kill buzz completely.

5.6 Linear and CFD based flutter results for Model1 and Model2

The aeroelastic effect of the oscillating flap when attached to the wing trailing edge is measured in this section. Linear calculations are performed using NASTRAN. The wing and the flap are included in the analysis with a total of 486 aerodynamic panels to calculate the aerodynamics. The Doublet Lattice Method is used in the subsonic flows and ZONA51 for supersonic flows. The first 5 natural modes including the flap mode of vibration are used in the aeroelastic analysis of Model 1 (See Section 2.2) whereas the first 4 natural modes are used for the aeroelastic analysis of Model 2. Figure 16 shows the flutter boundary of the two models calculated by linear methods and CFD.

The flutter velocity calculated by NASTRAN for Model1 has a big dip at Mach 1.05 and then increases. As the linear models are not able to predict shocks, this dip remains unexplained. One possibility is that linearised supersonic theories give negative damping for an aerofoil pitching along its leading edge at low supersonic Mach numbers. In the current case the flap is oscillating along its leading edge (the hinge line) and this might be the reason for the spurious flutter velocities of the wing between Mach numbers 1.05 and 1.4. The flutter velocities calculated by CFD on a coarse grid and using the Euler equations match the linear results in the low subsonic regions. There is a dip at Mach 0.9 due to the shock formation over the wing which is not predicted by NASTRAN. After Mach 0.95 the shock moves over the control surface and the oscillations due to buzz dominate the aeroelastic response. As buzz is shock driven the oscillations persist at even very low velocities (as low as 100 m/s). It was shown in Section 5.3 that the onset of buzz is sensitive to the initial impulse given to the flap. It was also shown that for the current case the buzz does not occur when the initial impulse is small at Mach 0.95. Hence it is possible to couple the wing bending and wing torsion mode by giving a small impulse to the wing bending mode at Mach 0.95 without exciting the flap mode. This is the reason a flutter velocity could be extracted at Mach 0.95 but not at higher Mach numbers where there is onset of buzz at a small impulse to the flap mode. To understand the dominance of shock effects at the upper transonic flow, Figure 17 shows the modal response of the 5 modes of Model 1 at the Mach 0.95 and dynamic pressure of 5.4 kPa . The freestream velocity is 125 m/s which is below the critical flutter velocity. When the initial impulse is given to the first wing bending mode the oscillations are damped. However when the impulse is given to the flap mode the wing starts to undergo a limit cycle oscillation involving all the modes. Figure 17(f) shows the modal response of all the modes at Mach 1.05. Here the wing undergoes limit cycle oscillation of all the modes even though the initial impulse was given to the first wing bending mode.

The flutter velocities calculated for Model 2 where the flap is held rigid shows a normal wing behaviour in both NASTRAN and CFD simulations. NASTRAN is unable to predict the transonic dip which is captured by CFD. Also the big dip in the flutter velocity predicted by NASTRAN when the flap is allowed to move in Model 1 is absent. A reasonable match between the CFD and linear results is obtained at subsonic and supersonic Mach numbers. As compared to Model 1 the flutter velocities are much higher which underscores the significance of the aeroelastic effects of control surfaces on the wing structure.

6 CONCLUSIONS

A method for simulation of 3D buzz was demonstrated. Apart from the prediction of the instability boundary, buzz parameters like amplitude, frequency and effect of damping were also measured using

the Euler and RANS equations. Buzz simulations using the Euler equations were performed on blended flaps and flaps with free edges and the flap response was found to be similar. A strong dependence of the buzz onset on the initial impulse was observed. From inviscid simulations it was concluded that although they can predict the onset of buzz, they cannot accurately predict the buzz parameters like amplitude and frequency. Flow separation over the oscillating flap has an influence on these parameters and hence viscosity effects need to be modelled. Consistent with experimental observations the amplitude of LCO predicted by the RANS equations was found to be sensitive to the Reynolds number and the reduced frequency of the flap.

The effect of control surface on the flutter of the wing was investigated and it was found to reduce the flutter velocity significantly even at subsonic flows as compared to a wing without a control surface. In transonic and supersonic flows the shock induced oscillations of the flap dominate the aeroelastic response of the wing dictating the frequency of oscillations.

The present work has looked into time marching simulation of a thin section wing where the flow is more or less attached at all Mach numbers and at low incidence angles. Future work can include geometries with thicker sections where the flow is detached when it reaches the flap hinge line. Buzz prediction using Hopf bifurcation to identify instability point is also proposed.

ACKNOWLEDGEMENTS

This work was supported by BAE SYSTEMS, Engineering and Physical Sciences Research Council, Ministry of Defence and Department of Trade and Industry, and forms part of the work program of the Partnership for Unsteady Methods in Aerodynamics (PUMA) Defence and Aerospace Research Partnership (DARP). The authors would also like to thank Dr. M. Tamayama of JAXA, Japan for his insight into the problem.

REFERENCES

- [1] R. Melville. "Nonlinear Simulation of F-16 Aeroelastic Instability". *AIAA Paper 2001-0570*, 2001.
- [2] B. B. Prananta, J. C. Kok, S. P. Spekreijse, M. H. Hounjet and J. J. Meijer. "Simulation of Limit Cycle Oscillation of Fighter Aircraft at Moderate Angle of Attack". *International Forum on Aeroelasticity and Structural Dynamics - Amsterdam*, June 4-6 2003.
- [3] C. Farhat, P. Geuzaine and G. Brown. "Application of a Three-field Nonlinear Fluid-structure Formulation to the Prediction of the Aeroelastic Parameters of an F-16 Fighter". *Computers & Fluids*, Vol.32(3):pp.3–29, 2002.
- [4] M. A. Woodgate, K. J. Badcock, A. M. Rampurawala, D. Nardini and M. J. Henshaw. "Aeroelastic Calculations for the Hawk Aircraft Using the Euler Equations". *To appear in Journal of Aircraft*, 2005.
- [5] N. C. Lambourne. "Control Surface Buzz. *Aircraft Research Council R & M*, No. 3364, 1964.
- [6] Y. Nakamura. "Some Contributions on a Control Surface Buzz at High Subsonic Speeds". *Journal of Aircraft*, Vol.5(2):pp. 118, 1968.
- [7] Y. Nakamura and L. Woodgate. "Effects of Reynolds Number and Frequency Parameter on Control Surface Buzz at High Subsonic Speeds". *Aeronautical Research Council R & M*, No. 3702, 1972.
- [8] O. O. Bendiksen. "Nonclassical Aileron Buzz in Transonic Flow". *34th AIAA/ASME/ASCE/AHS/ASC Structures, Structural Dynamics and Materials Conference*, (AIAA Paper 93–1479), April 1993.
- [9] J. L. Steger and H. E. Bailey. "Calculation of Transonic Aileron Buzz". *AIAA Journal*, Vol.18(3):pp. 249–255, 1980.
- [10] A. L. Erickson and J. D. Stephenson. "A Suggested Method for Analyzing for Transonic Flutter of Control Surfaces Based on Available Data". *NACA RM A7F30*, 1947.
- [11] D. F. Fuglsang, L. O. Brase and S. Agarwal. "A Numerical Study of Control Surface Buzz Using Computational Fluid Dynamics Methods". *10th AIAA Applied Aerodynamics Conference*, (AIAA Paper 92–2654), June 1992.
- [12] M. Tamayama, T. A. Weisshaar and J. Nakamichi. "Unsteady Shock Wave Motions on a Thin Airfoil at Transonic Speeds Caused by an Aileron Oscillation". *International Forum on Aeroelasticity and Structural Dynamics - Amsterdam*, June 4–6 2003.
- [13] G. Yang and S. Obayashi. "Aileron Buzz Simulation Using an Implicit Multiblock Aeroelastic Solver". *Journal of Aircraft*, Vol.40(3):pp. 580–589, 2003.
- [14] K. J. Badcock, M. A. Woodgate and B. E. Richards. "Elements of Computational Fluid Dynamics on Block Structured Grids using Implicit Solvers". *Progress in Aerospace Sciences*, Vol.36:pp. 351–392, 2000.

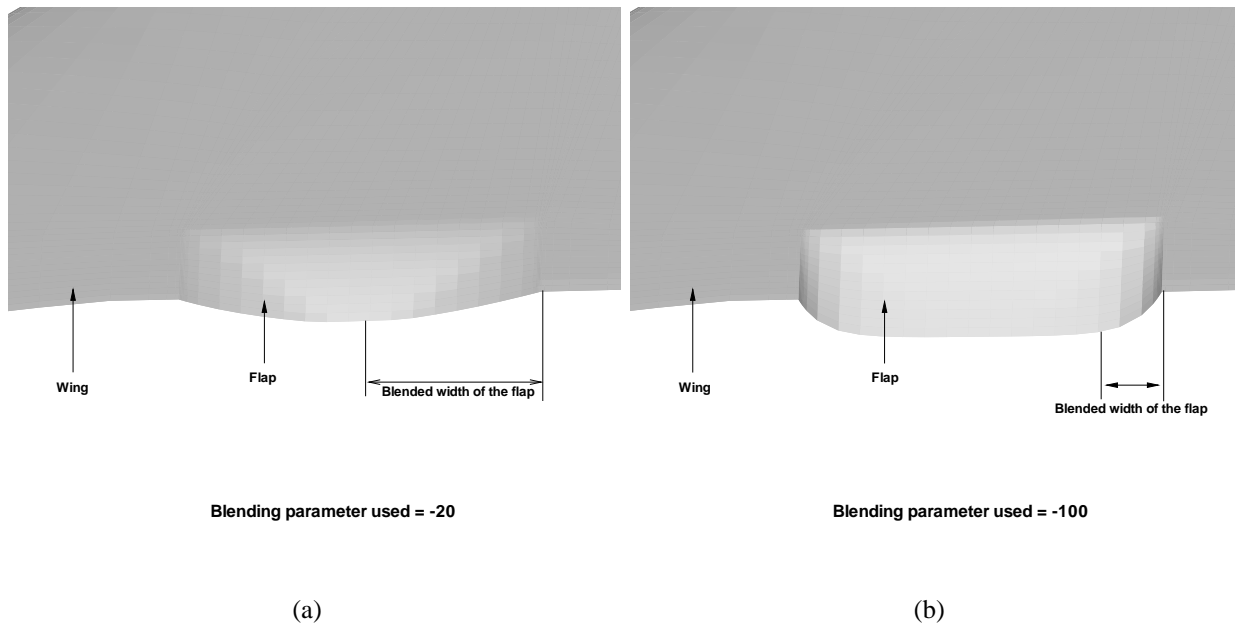


Figure 1: Transformed flap mode using two different values of blending parameter

- [15] G. S. L. Goura. "Time marching analysis of flutter using Computational Fluid Dynamics". PhD thesis, University of Glasgow, 2001.
- [16] G. S. L. Goura, K. J. Badcock, M. A. Woodgate and B. E. Richards. "Implicit Method for the Time Marching Analysis of Flutter". *Aeronautical Journal*, Vol.105:pp. 199–214, April 2001.
- [17] W. J. Gordon and C. A. Hall. "Construction of Curvilinear Coordinate Systems and Applications to Mesh Generation". *International Journal of Numerical Methods in Engineering*, Vol.7:pp. 461–477, 1973.
- [18] C. L. Fenwick and C. B. Allen, Development. "Validation of Sliding Grid Technology for Time-Domain Aeroservoelastic Simulations". *23rd AIAA Applied Aerodynamics Conference*, (AIAA Paper 2005–4844), June 2005.
- [19] G. H. Klopfer and S. Obayashi. "Virtual Zone Navier-Stokes Computations for Oscillating Control Surfaces". AIAA Paper 1993-3363, 1993.
- [20] A. M. Rampurawala K. J. Badcock and B. E. Richards. "Intergrid Transformation for Aircraft Aeroelastic Simulations". *AIAA Journal*, Vol.42(9):pp. 1936–1939, September 2003.
- [21] H. Matsushita M. Tamayama, K. Saitoh and J. Nakamichi. "NAL SST Arrow Wing with Oscillating Flap". *RTO Report*, RTO-TR-26 AC/323(AVT)TP/19, October 2000.
- [22] A. M. Rampurawala and K. J. Badcock. "Treatment of Forced Flap Motions for Aeroelastic Simulations of an Arrow Wing". *23rd AIAA Applied Aerodynamics Conference*, (AIAA Paper 2005–4962), June 2005.

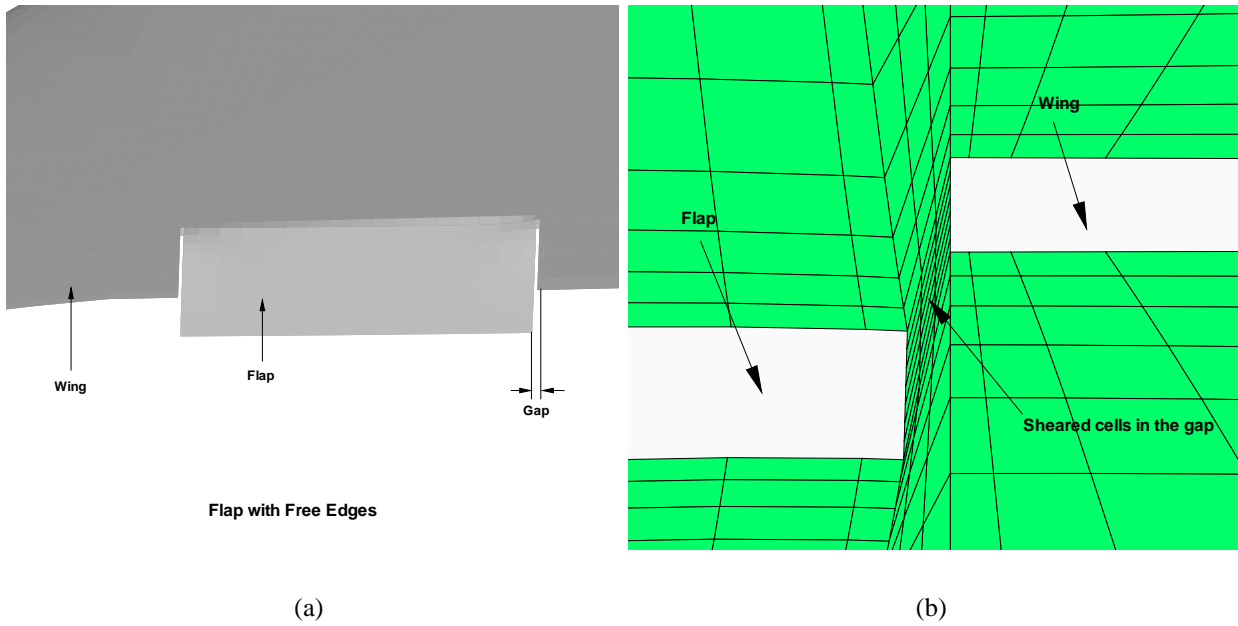


Figure 2: Transformed flap mode of a flap with free edges

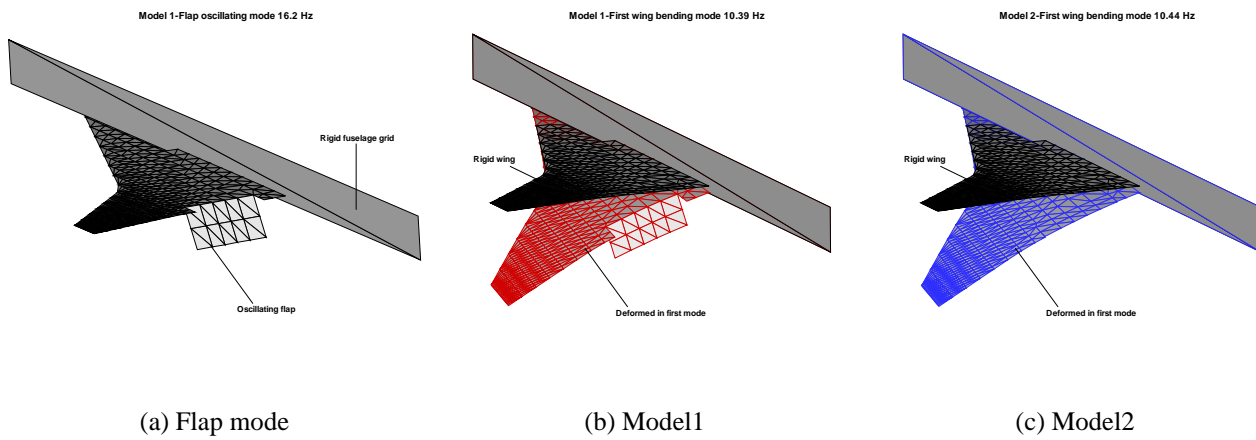


Figure 3: Structural models with the flap oscillation mode and the first wing bending mode

Mode	Frequency (Hz)- Model 1	Frequency (Hz)-Model 2
Wing bending	10.39	10.44
Flap Oscillation	16.202	-
Wing Torsion	44.24	44.13
Second Wing Bending	53.89	50.23
Second Wing Torsion	89.06	88.80

Table 1: Natural frequencies of the model

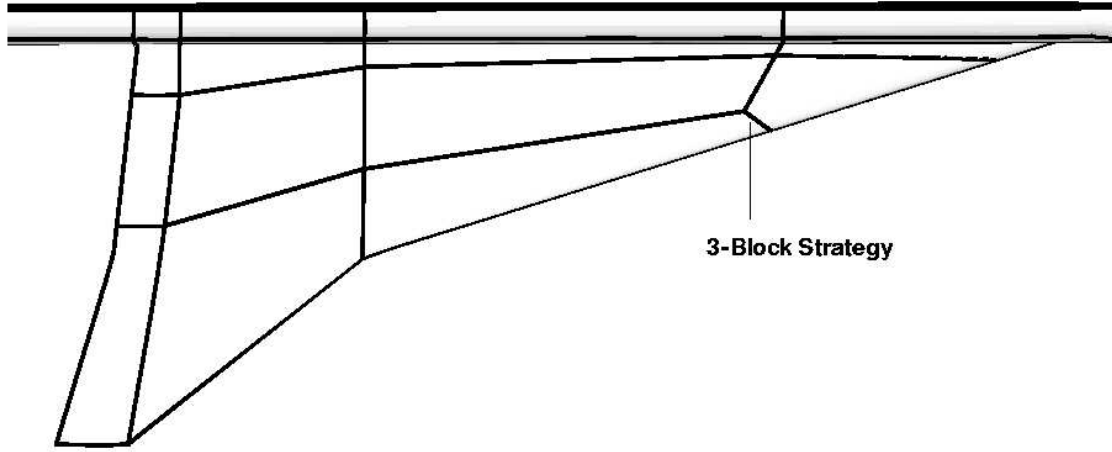


Figure 4: 3-block strategy to prevent a collapsed point at the leading edge of the wing root

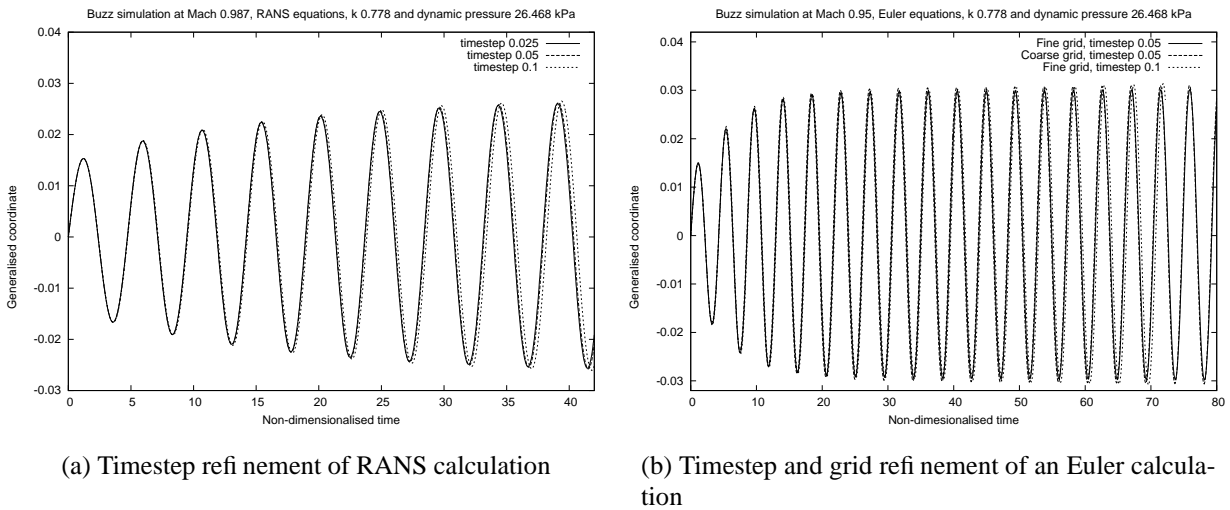


Figure 5: Timestep and grid refinement calculations

Mach No.	0.9	0.91	0.92	0.93	0.95	0.98	1.1	1.2	1.3	1.4
Euler blended	No	No	Yes	Yes	Yes	Yes	Yes	Yes	No	-
Euler gap	No	No	No	Yes	Yes	Yes	Yes	Yes	No	-
Viscous	No	-	No	-	Yes	Yes	Yes	Yes	Yes	Maybe

Table 2: Buzz prediction at various Mach numbers by different models

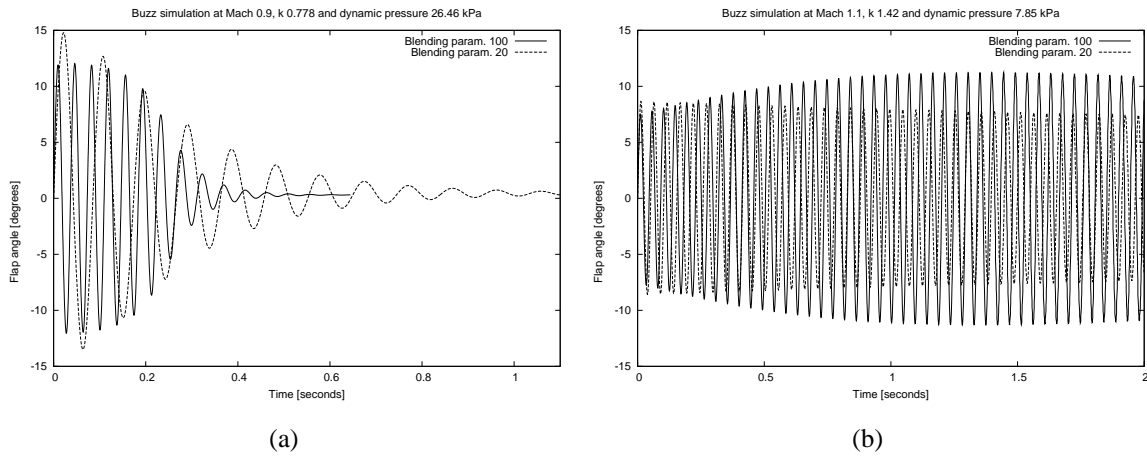


Figure 6: Flap response at different values of blending parameter

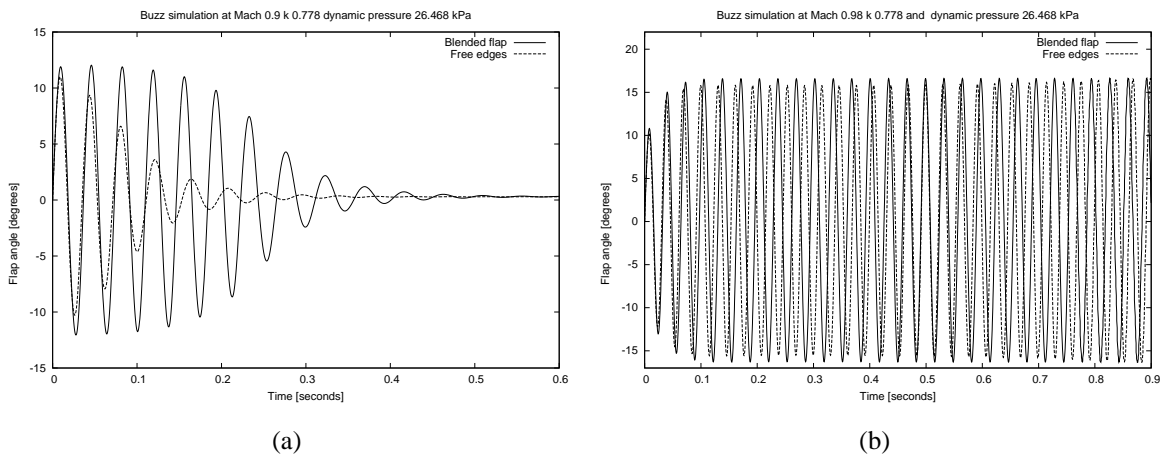


Figure 7: Flap response of blended and free flaps at different Mach numbers

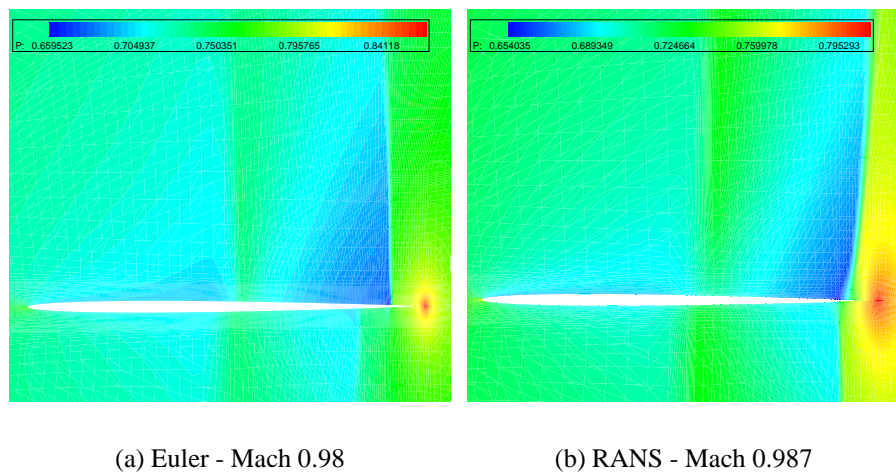
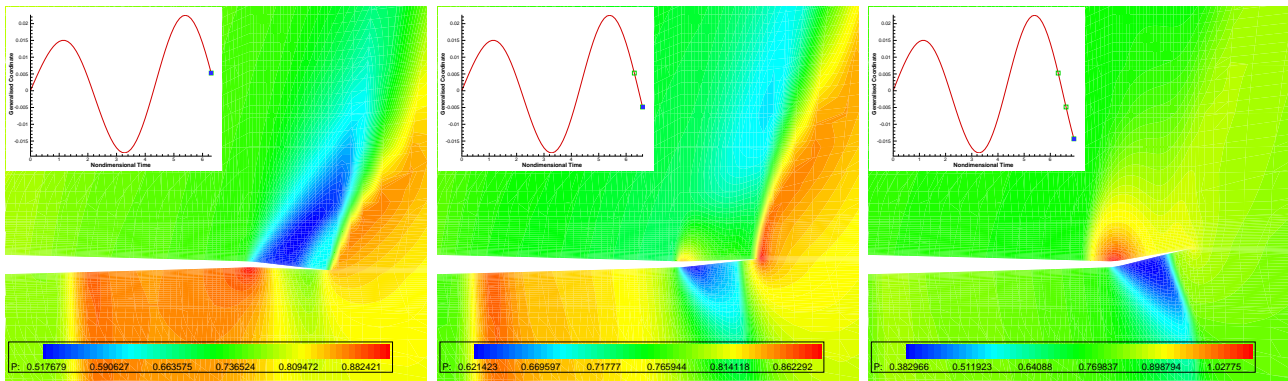


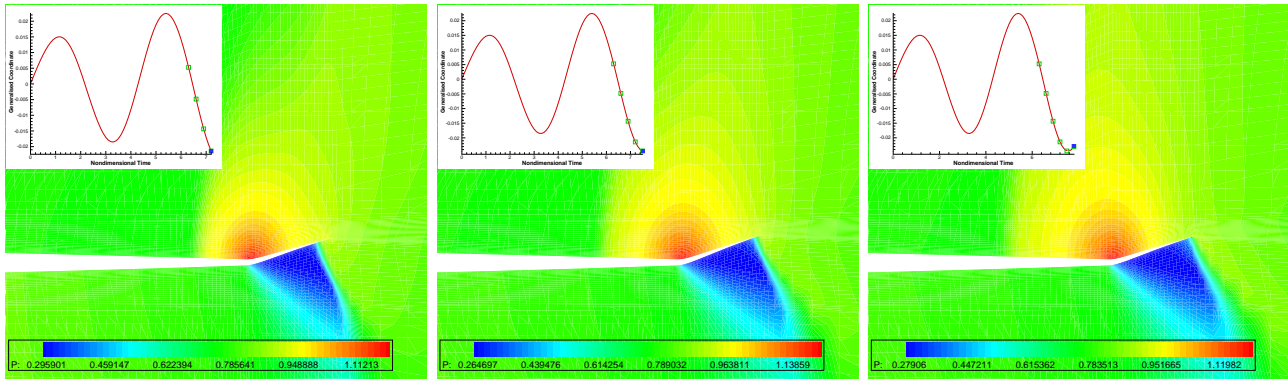
Figure 8: Steady pressure contours for Euler and RANS cases at a slice taken at 38.4% span.



(a)

(b)

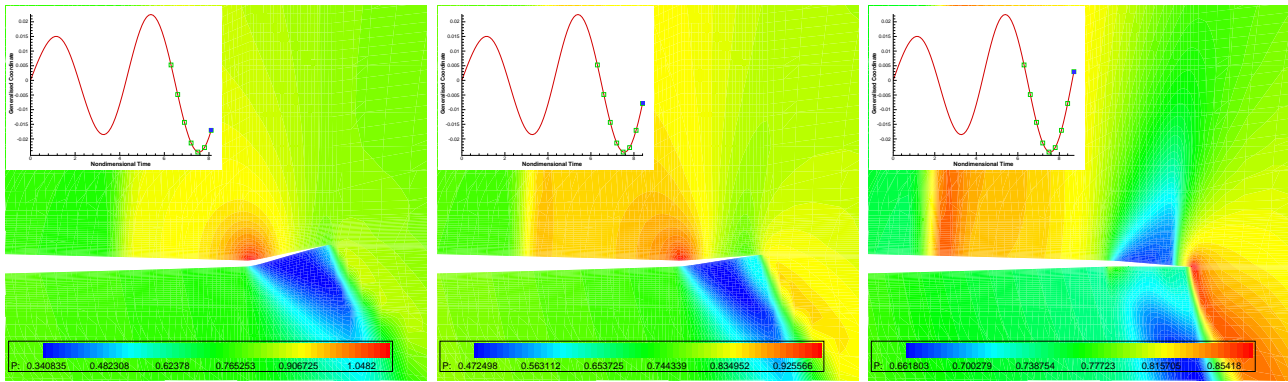
(c)



(d)

(e)

(f)

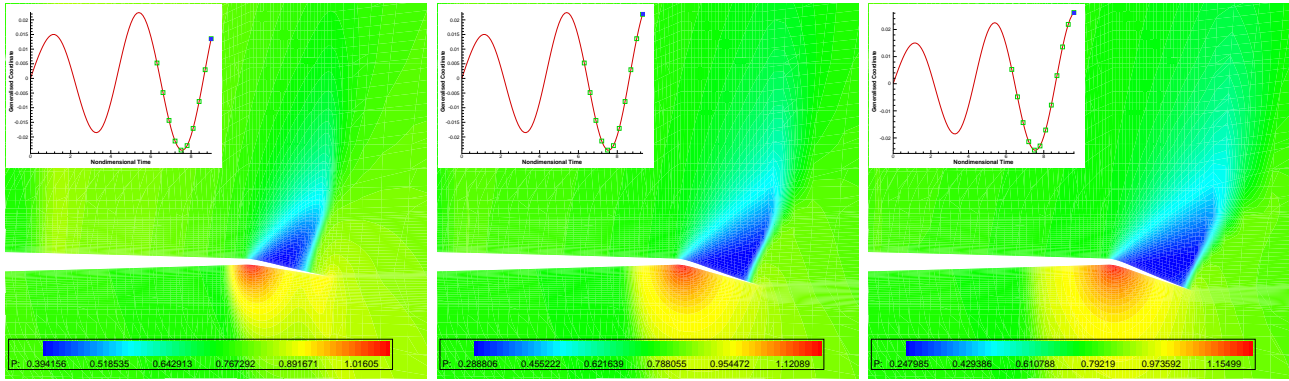


(g)

(h)

(i)

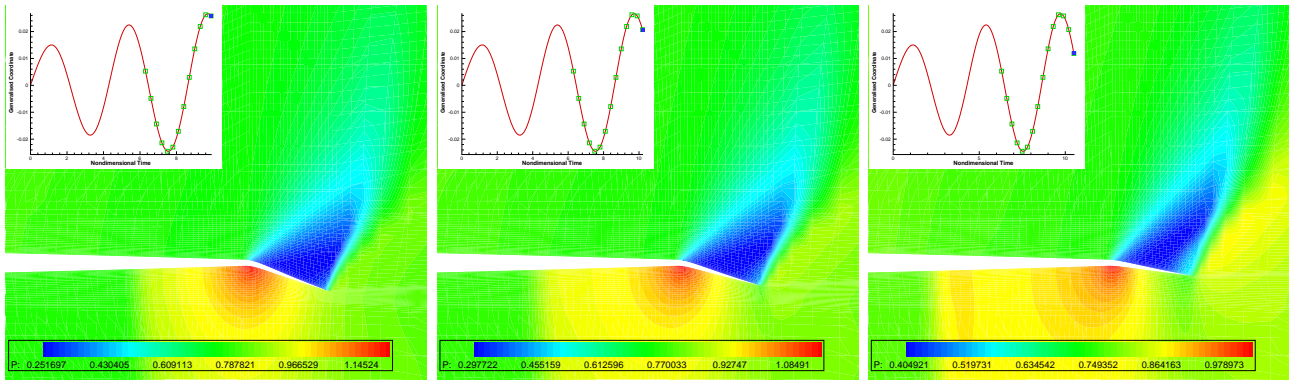
Figure 9: Unsteady pressure contours during a single buzz cycle (cont.)



(a)

(b)

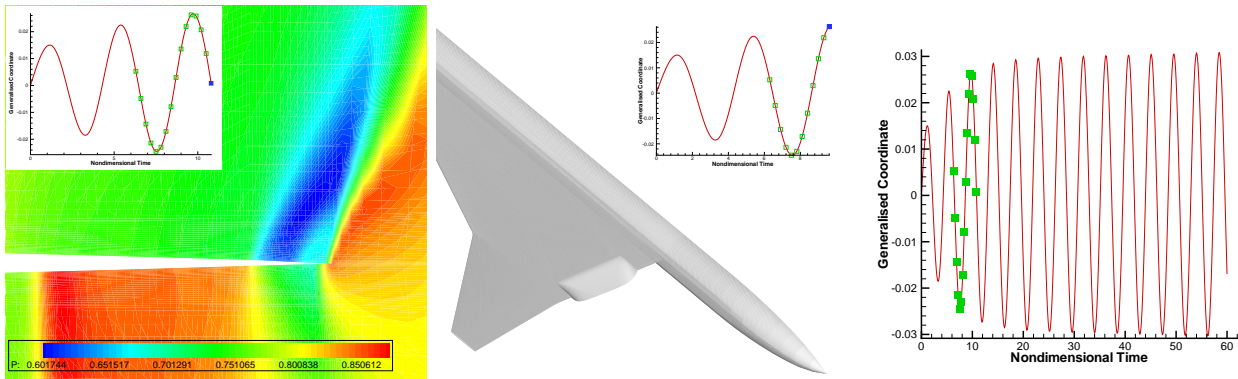
(c)



(d)

(e)

(f)

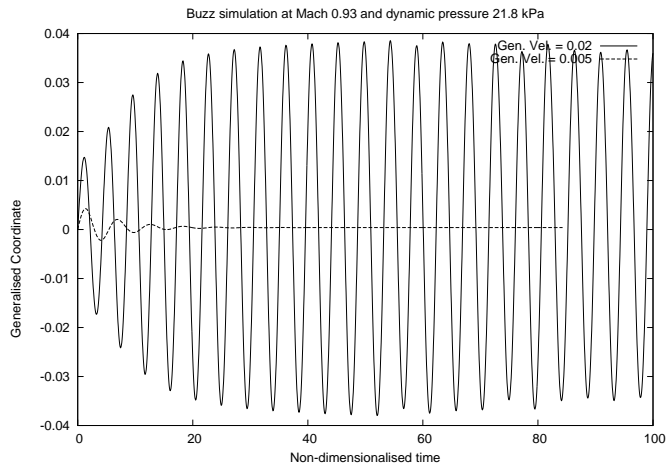


(g)

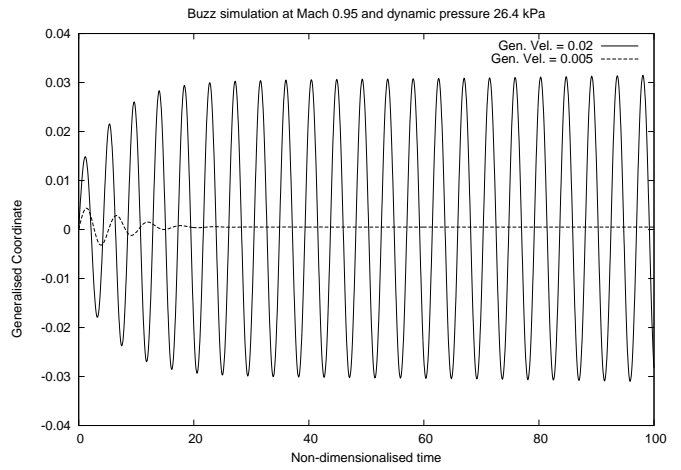
(h)

(i)

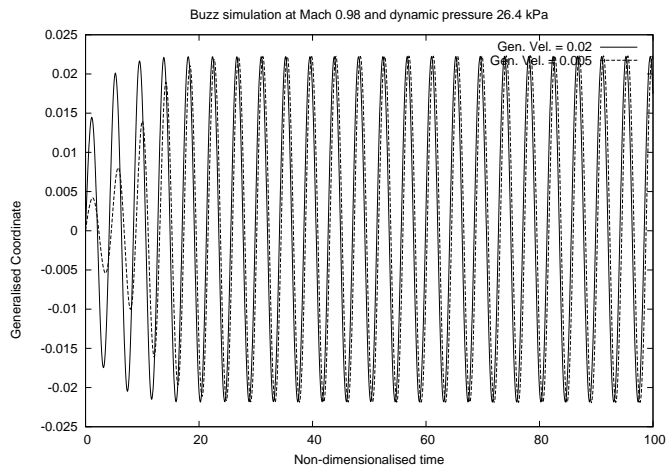
Figure 10: Unsteady pressure contours during a single buzz cycle



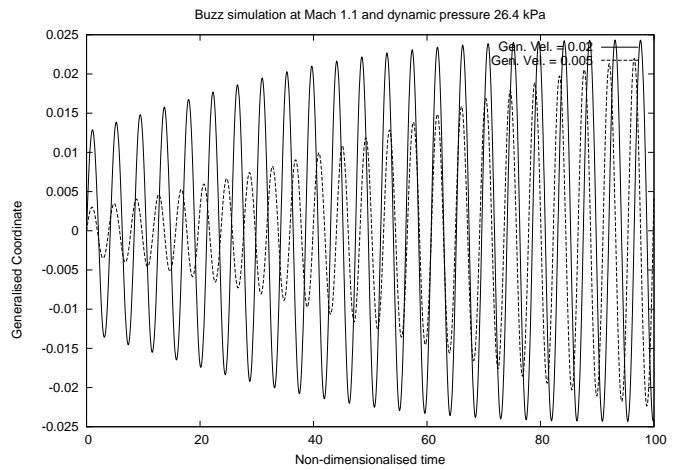
(a)



(b)

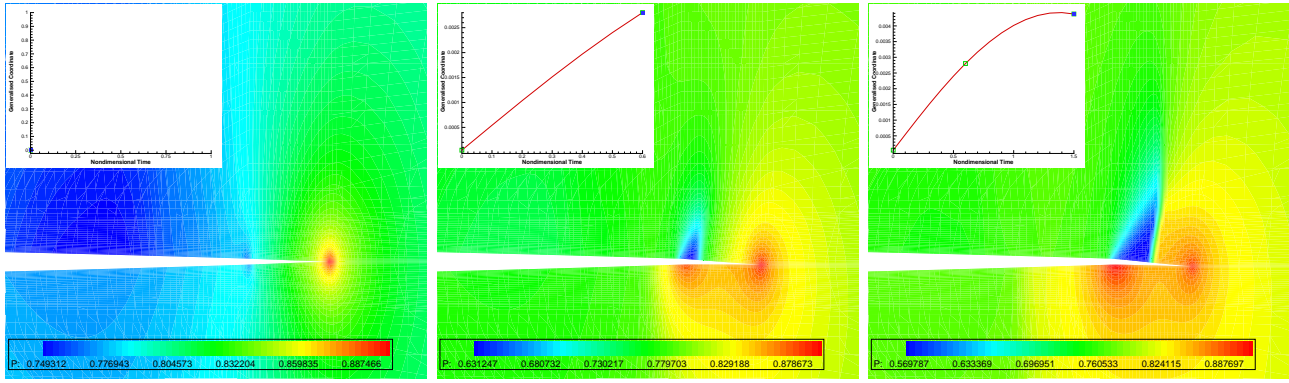


(c)



(d)

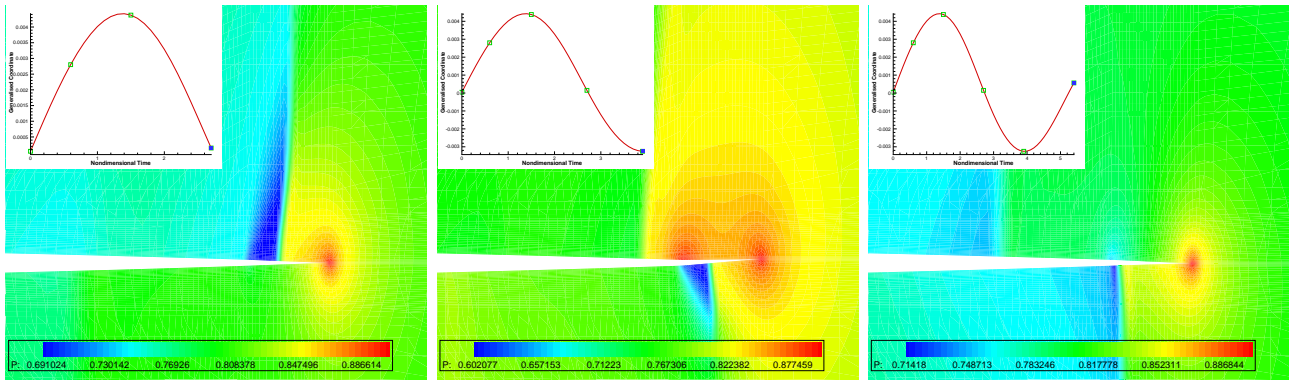
Figure 11: Dependence of buzz on initial impulse at Mach numbers 0.9 - 0.95



(a)

(b)

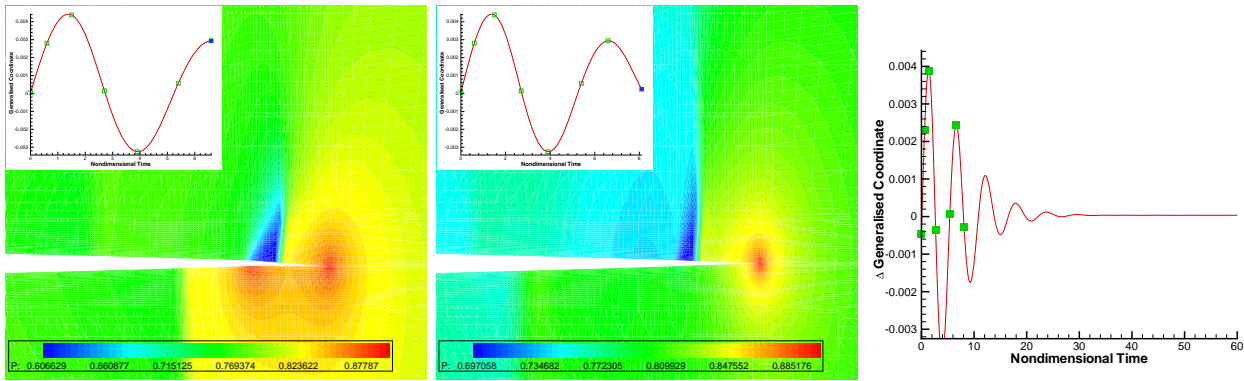
(c)



(d)

(e)

(f)

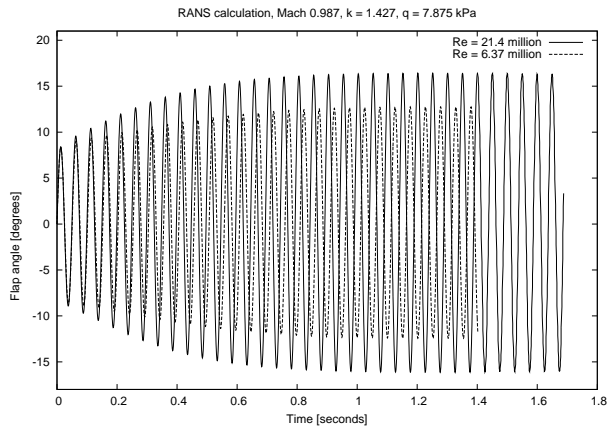


(g)

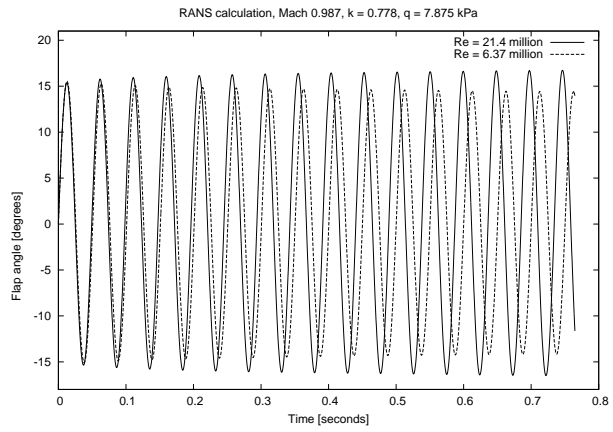
(h)

(i)

Figure 12: Unsteady pressure contours of decaying buzz cycle

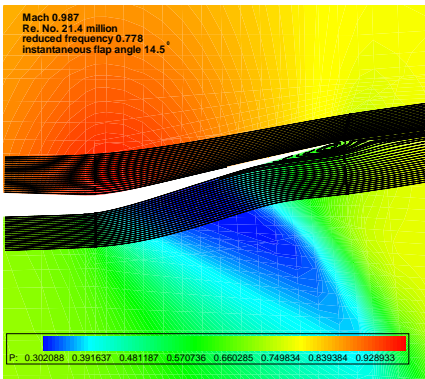


(a)

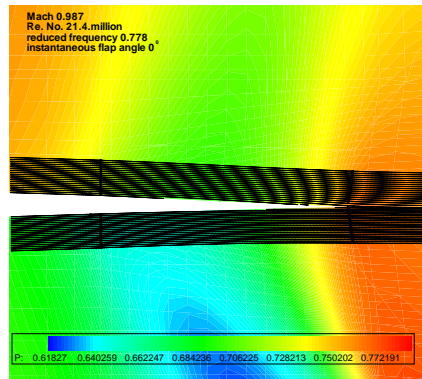


(b)

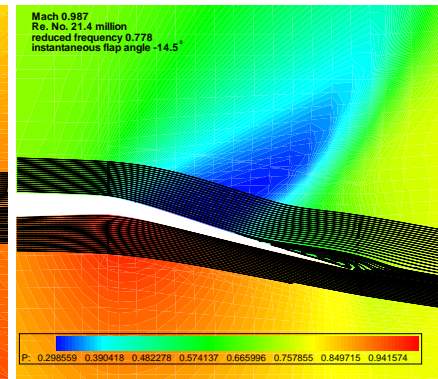
Figure 13: Dependence of buzz amplitude and frequency on the Reynolds number



(a)



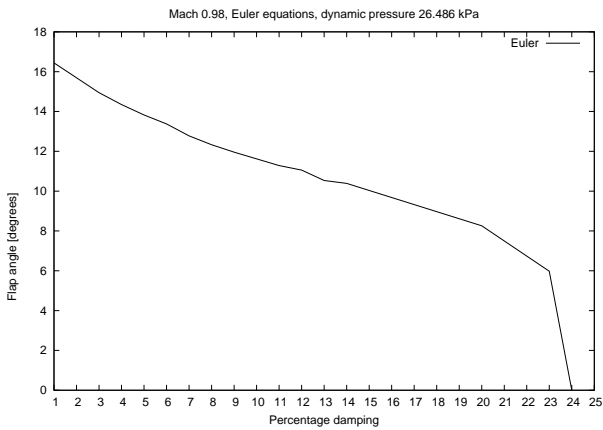
(b)



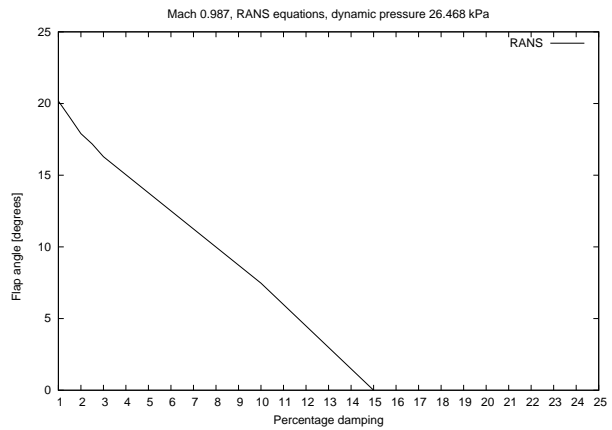
(c)

Figure 14: Separation on the flap along a buzz cycle for a case at 0.6° incidence

E

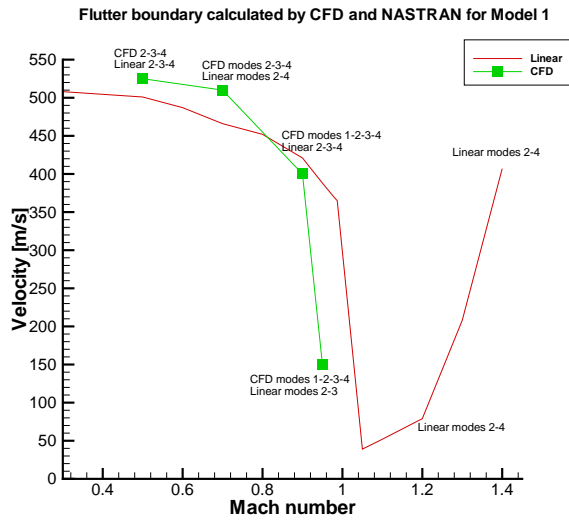


(a)

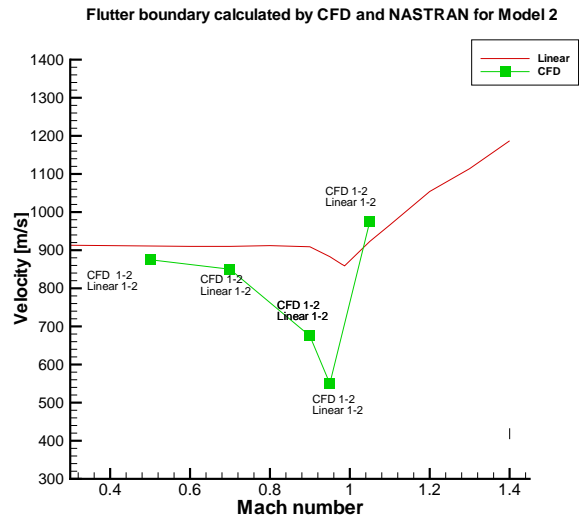


(b)

Figure 15: Effect of damping on buzz amplitude

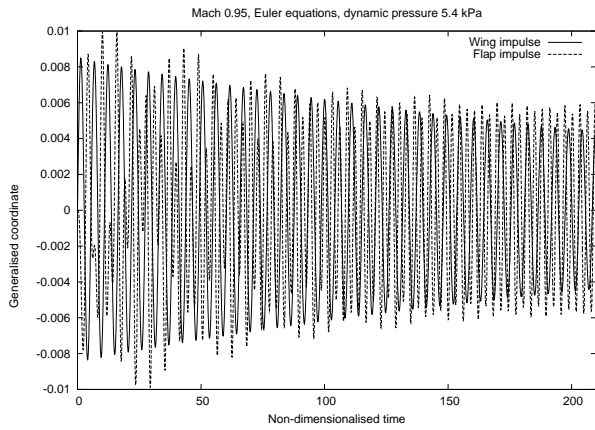


(a)

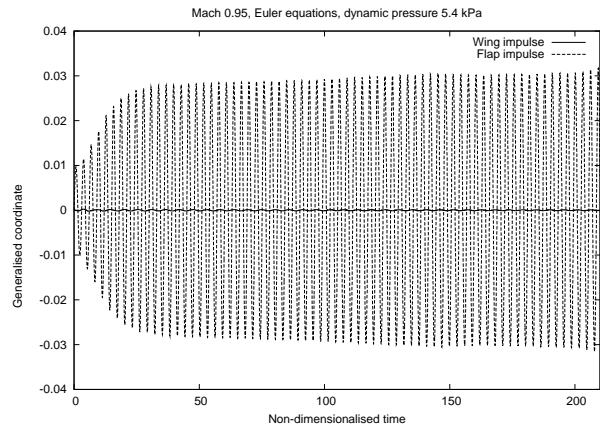


(b)

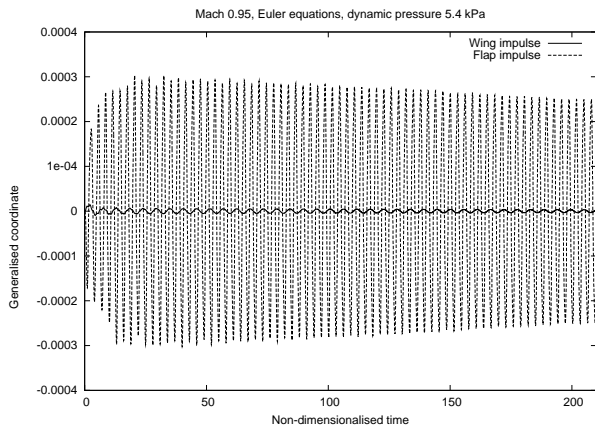
Figure 16: Flutter boundary along with the interacting modes calculated by NASTRAN and PMB



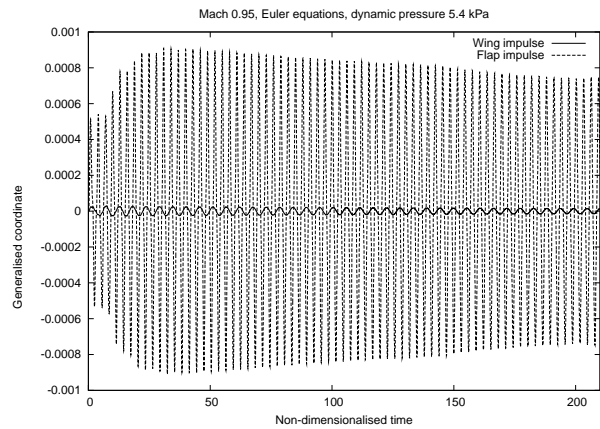
(a) Mode 1



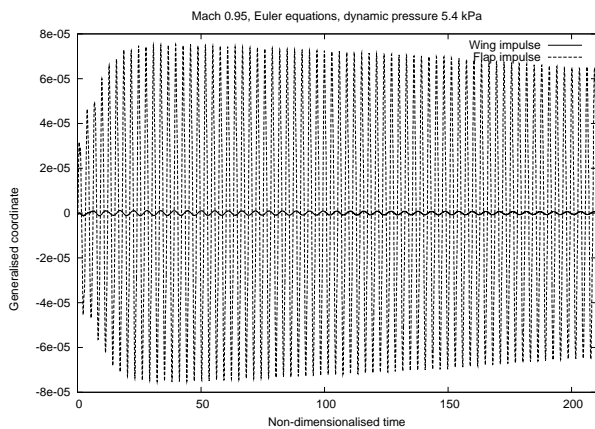
(b) Mode 2



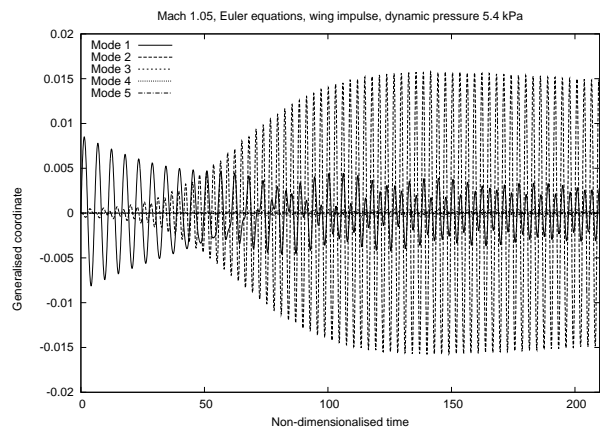
(c) Mode 3



(d) Mode 4



(e) Mode 5



(f) Modal response of all 5 modes at Mach 1.05

Figure 17: Domination of shock induced aeroelastic response at higher transonic Mach numbers